Bulletin of the Seismological Society of America, Vol. 100, No. 5B, pp. 2440–2449, November 2010, doi: 10.1785/0120090245

Analysis of Horizontal Strong-Motion Attenuation in the Great 2008 Wenchuan Earthquake

by Xiao Jun Li, Lang Liu, Yu Shi Wang, and Tian Yu

Abstract A large number of strong-motion records were obtained by the National Strong-Motion Observation Network System (NSMONS) of China for the Wenchuan earthquake. There are 1350 components of strong-motion records from the mainshock at 455 stations. In these stations, 164 stations are located in the range of rupture distance within 400 km and 37 stations are within 100 km. The largest peak ground acceleration is 957.8 Gal from the Wolong station in the hanging wall area with rupture distance of 23 km. The records from 164 stations in the range of rupture distance within 400 km are used in this study to investigate the hanging wall/footwall effects, directivity effects, and attenuation characteristics of ground motions from the Wenchuan earthquake. The characteristics of ground motion attenuations are compared in four subareas: hanging wall area, footwall area, forward directivity area, and backward directivity area. The study results show a clear hanging wall/footwall effect in near-fault ground motions within a rupture distance of 40 km, but it appears only in the peak ground acceleration and components at short periods below 1.0 s, and a strong forward directivity effect appears in ground motions over the whole range of rupture distance and period. Furthermore, the fitting attenuation curves of the peak ground acceleration and spectral accelerations of ground motions from the Wenchuan earthquake are compared with the predicted curves by an empirical attenuation model in the hanging wall and footwall areas.

Introduction

In number and density of strong-motion observation stations, the mainland of China was seriously behind the United States, Japan, Iran, and Mexico before 2000 (Gao, *et al.*, 2001; Nozu, 2004; Li, *et al.*, 2006; Zhou, 2006). It could not meet the needs of research and engineering constructions in China. In order to change the situation, the nation provided funds to implement the Project of China Digital Strong-Motion Observation Network. After five years of construction, the project was completed (Earthquake Disaster Prevention and Mitigation Division of China Earthquake Administration, 2008); the National Strong-Motion Observation Network System (NSMONS) of China was established, forming a large scale of strong-motion observation networks in the mainland of China (Li, *et al.*, 2006). The NSMONS began trial operation in early 2007 and entered formal operation in March 2008.

The Wenchuan earthquake (M_w 7.9) occurred in Sichuan Province, China, on 12 May 2008. The fault rupture initiated in the southern Longmen Shan and propagated unilaterally toward the northeast for about 300 km (Wang, *et al.*, 2008; Xu, Wen, Yu, *et al.*, 2009, Xu, Yu, Chen, *et al.*, 2009). During the Wenchuan earthquake, the network system (NSMONS) obtained 1350 components of strong-motion records from the mainshock; this included records from 437 free-field stations in 17 provinces, municipalities, and autonomous regions, 1 array (8 stations) for topographical effect observation in Sichuan Province, and 2 temporary arrays (10 monitoring points) for structural response observation in the Kunming mobile observatory (Li, Zhou, Yu, *et al.*, 2008, Li, Zhou, Huang, *et al.*, 2008). The locations of the free-field stations for mainshock recordings are shown in Figure 1. After the mainshock, 59 mobile instruments were quickly deployed to record ground motions and structural responses from strong aftershocks, and a large number of aftershock records also were obtained. The strong-motion records from the mainshock and aftershocks provide basic data for researches on the earthquake ground motions and structural responses.

Strong-Motion Records Used in This Study

In this study, the strong-motion records of the mainshock in the range of 400 km within the rupture distance, including 328 horizontal components from 164 free-field stations as shown in Figure 2, are used to investigate the hanging wall/footwall effect, directivity effect, and attenuation characteristics of ground motions from the Wenchuan

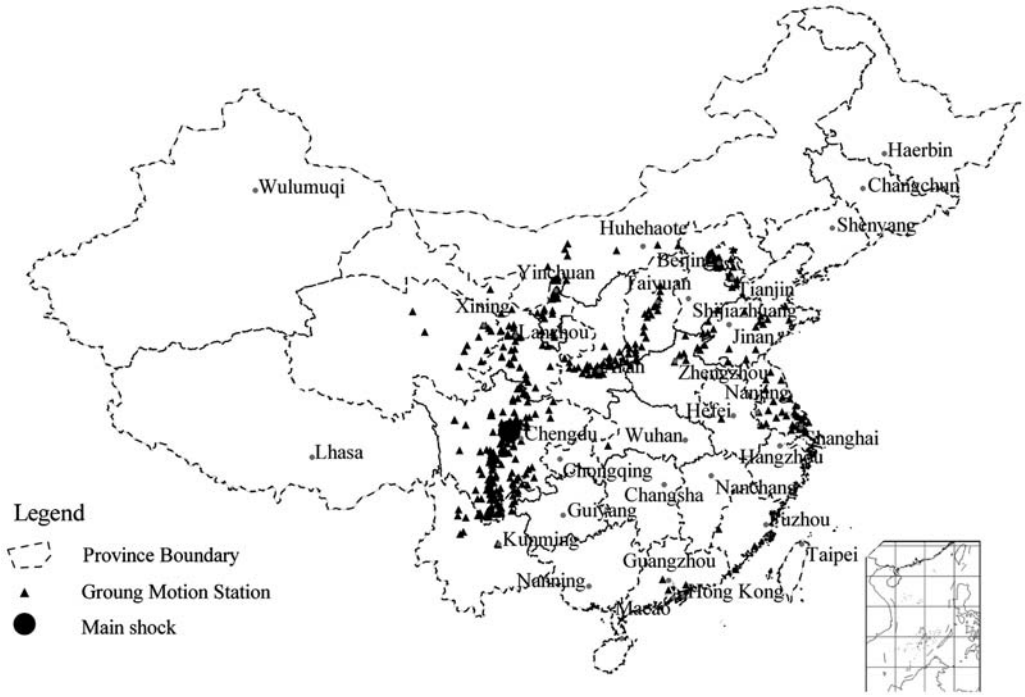

Figure 1. Location of strong-motion stations that recorded the mainshock of the Wenchuan earthquake

earthquake. The strong-motion records were obtained from the China Strong-Motion Net Center (see the Data and Resources section). Because the fault rupture of the Wenchuan earthquake initiated in the southern Longmen Shan and propagated unilaterally toward the northeast for about 300 km, there are large differences in the source directivity that may produce a strong rupture directivity effect on the ground motion, particularly in the near-fault area. The Wenchuan earthquake generated two surface rupture zones, the Beichuan rupture zone and the Hanwang rupture zone as shown in Figure 2, in which the Beichuan rupture zone along the Yingxiu–Beichuan fault is a main surface rupture zone. In this study, the Yingxiu–Beichuan fault is considered the fault that caused the Wenchuan earthquake; the fault model

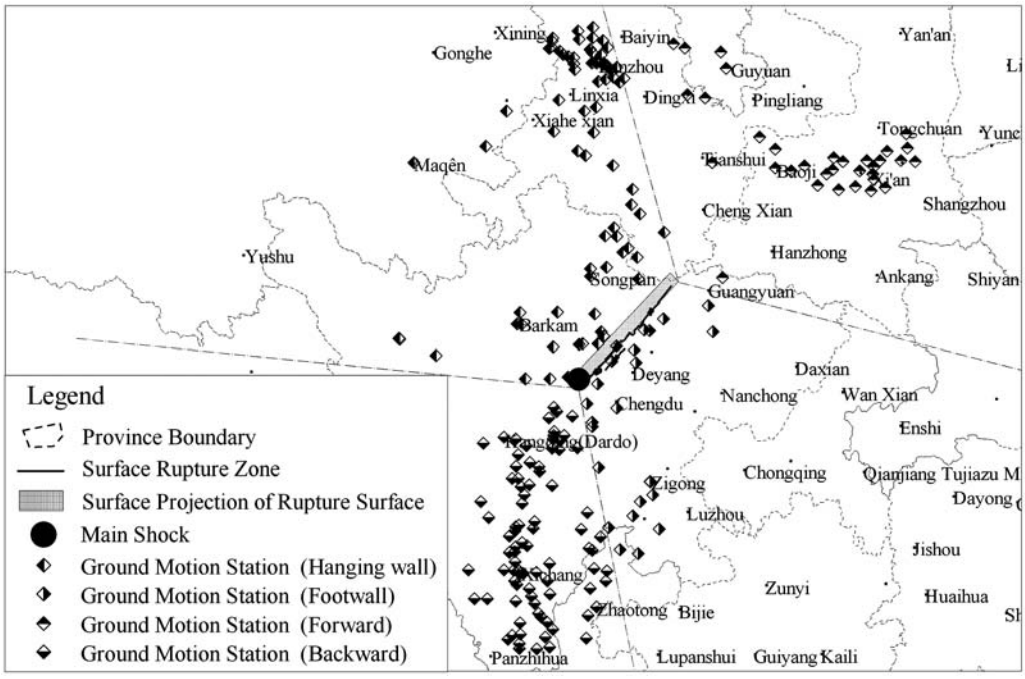

Figure 2. Distribution of the strong-motion stations that recorded the mainshock of the Wenchuan earthquake used in this study.

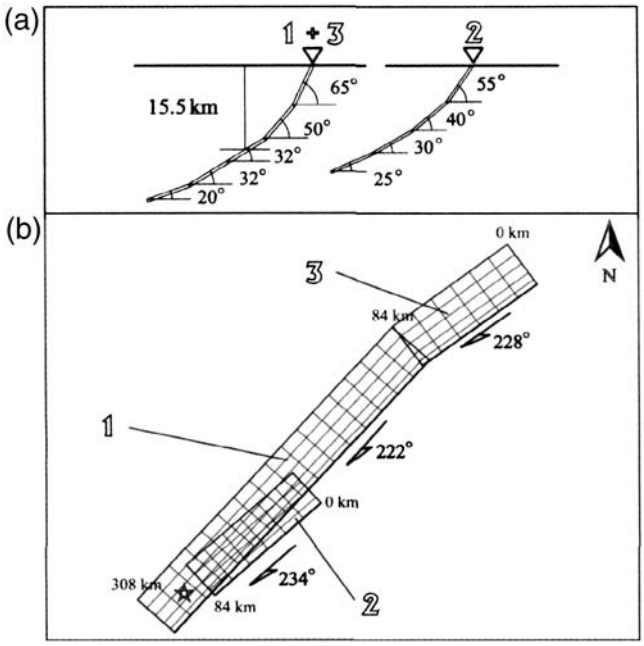

Figure 3. Wang's fault model for the Wenchuan earthquake (Wang *et al.*, 2008). Model unit 1 and 3 modeling the Yingxiu–Beichuan fault, and unit 2 modeling the Guanxian-Jiangyou fault. (a) Cross section of the fault model; (b) surface projection of the fault model.

proposed by Wang (Wang *et al.*, 2008), as shown in Figure 3, is adopted to determine the rupture distance of the strong-motion observation station. The rupture distance is defined as the shortest distance from the strong-motion observation station to the rupture surface in this study. With reference to the surface rupture zone of the Yingxiu–Beichuan fault, four study subareas, including the hanging wall area, footwall area, forward directivity area, and backward directivity area, are defined as shown in Figure 2 to investigate the hanging wall/footwall effect, directivity effect, and attenuation characteristics of ground motions. Table 1 shows the numbers of the stations versus rupture distance in different subareas. There are 49, 31, 18, and 66 stations in the hanging wall, footwall, forward directivity, and backward directivity areas, respectively. There are a number of stations in the hanging wall and footwall areas, but only a few stations in the forward directivity and backward directivity areas in the range of rupture distance within 100 km.

Among the records, the largest peak acceleration was recorded at the Wolong station in the hanging wall area with a rupture distance of 23 km, whose peak accelerations were recorded in the east–west (EW), north–south (NS), and up–down (UD) directions as 957.7 Gal, 652.9 Gal, and 948.1 Gal, respectively. The nearest station to the surface rupture zone is the Qingping station in the footwall area with a rupture distance of 3 km; the peak accelerations recorded in the EW, NS, and UD directions are 824.1 Gal, 802.7 Gal, and 622.9 Gal, respectively. Two other stations very near to surface rupture zone are the Bajiao and the Zengjia stations in the footwall area with rupture distances of 10 km and 12 km, respectively.

Site classes of stations in this study are divided based on the Chinese site classification and investigated based on the site condition of the stations, such as the thickness and shear velocity of the overlying soils. As shown in Table 1, most of the stations are located at site class II, and only 16 and 1 of the 164 stations are located at site classes I and III, respectively.

Figures 4–8 show the distribution of horizontal peak ground accelerations and spectral accelerations at periods of 0.3 s, 1.0 s, 3.0 s, and 10.0 s versus the rupture distance from the Wenchuan earthquake records. The peak ground accelerations and spectral accelerations from the stations with site classes I and III are also shown in these figures.

Table 1
The Number of the Stations versus Rupture Distance in Different Subareas

Subarea	Rupture Distance (km)	Number of Stations			
		Site Class II	Site Class I	Site Class III	Total
Hanging wall	0–50	7	2	0	49
	51–100	9	1	0	
	101–200	9	0	0	
	201–400	20	0	1	
Footwall	0–50	7	2	0	31
	51–100	3	1	0	
	101–200	2	0	0	
	201–400	13	3	0	
Forward directivity	0–50	0	0	0	18
	51–100	1	0	0	
	101–200	0	0	0	
	201–400	15	2	0	
Backward directivity	0–50	0	0	0	66
	51–100	3	1	0	
	101–200	16	2	0	
	201–400	42	2	0	
Total	0–400	147	16	1	164

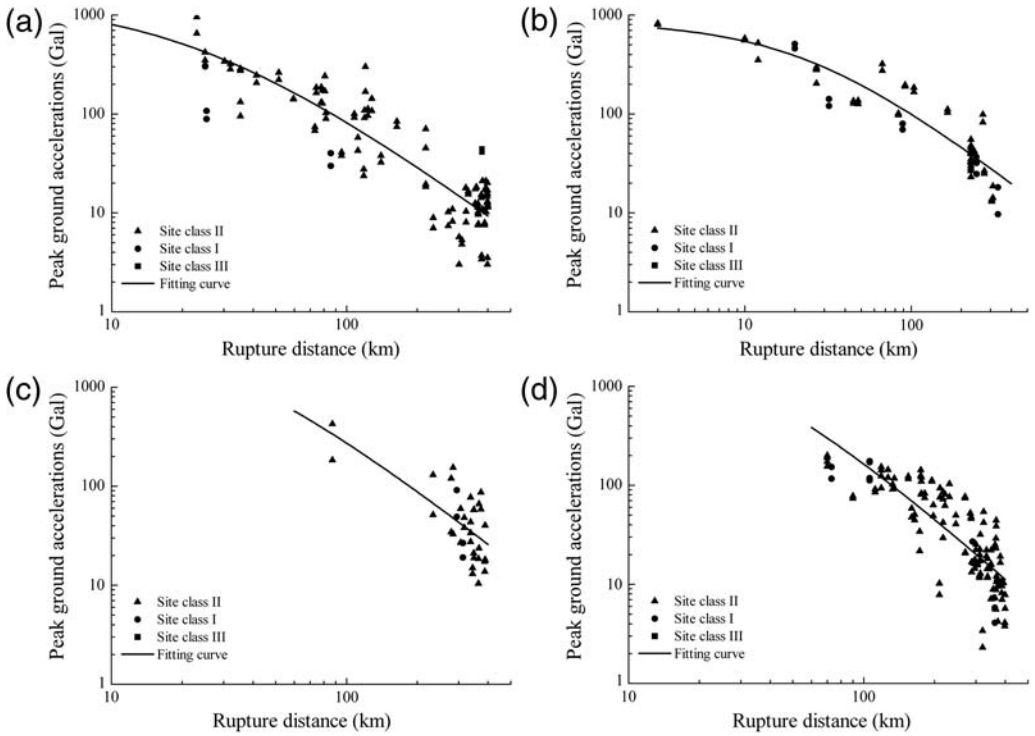

Figure 4. Peak ground accelerations versus rupture distance from horizontal components of the Wenchuan earthquake records in different subareas and for different site conditions, and fitting attenuation curves. (a) Hanging wall area; (b) footwall area; (c) forward directivity area; (d) backward directivity area.

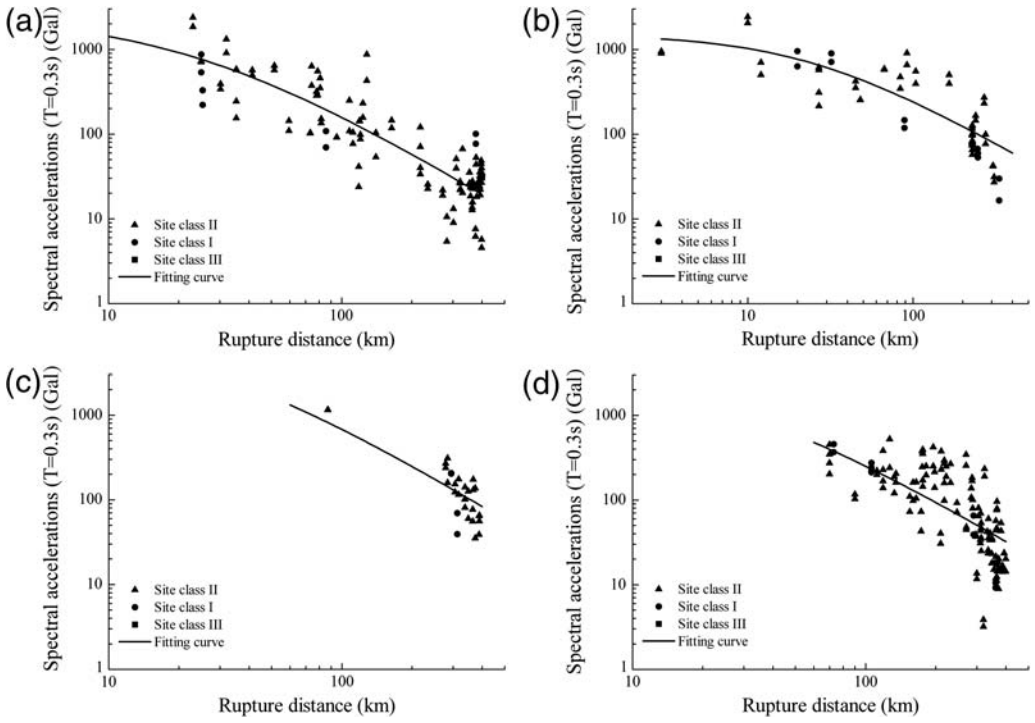

Figure 5. Spectral accelerations at period of 0.3 s versus rupture distance from horizontal components of the Wenchuan earthquake records in different subareas and for different site conditions, and fitting attenuation curves. (a) Hanging wall area; (b) footwall area; (c) forward directivity area; (d) backward directivity area.

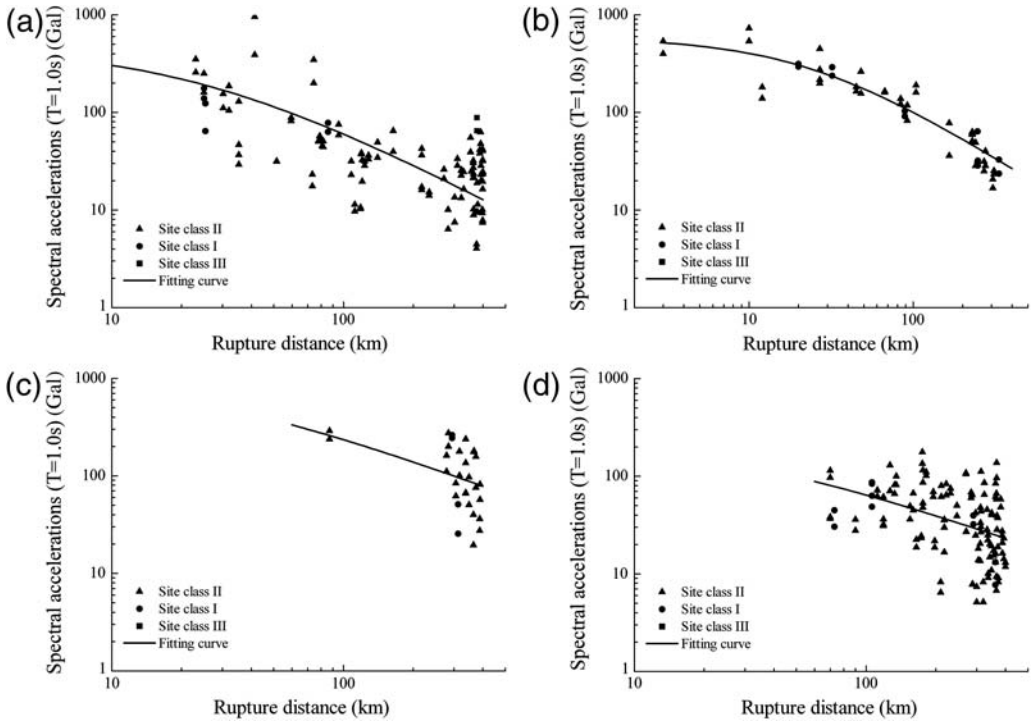

Figure 6. Spectral accelerations at period of 1.0 s versus rupture distance from horizontal components of the Wenchuan earthquake records in different subareas and for different site conditions, and fitting attenuation curves. (a) Hanging wall area; (b) footwall area; (c) forward directivity area; (d) backward directivity area.

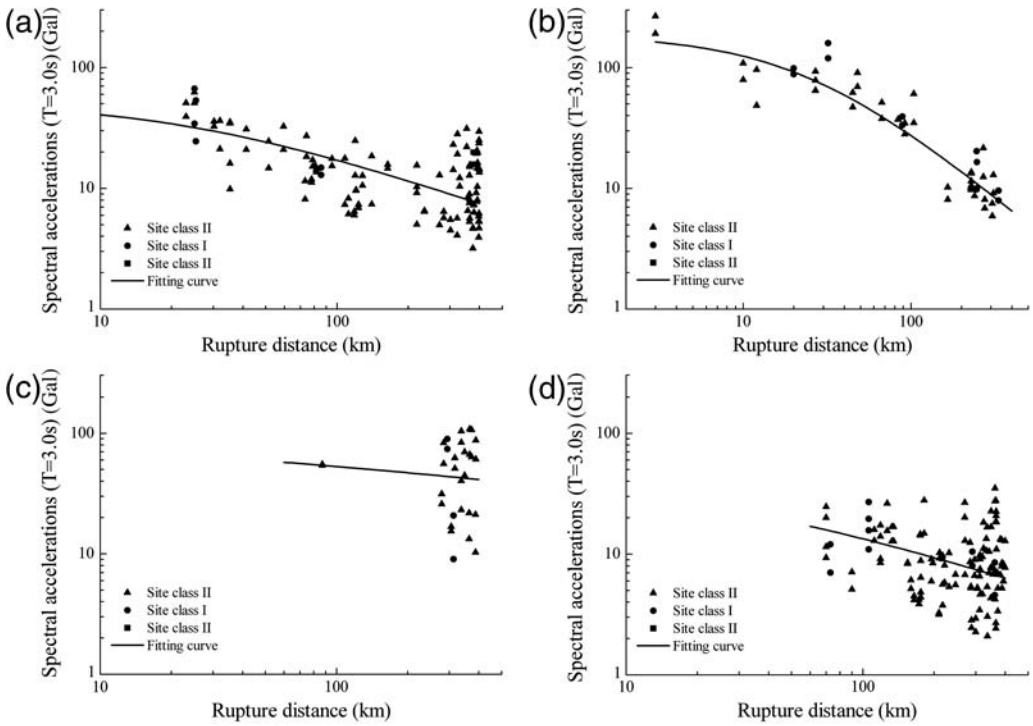

Figure 7. Spectral accelerations at period of 3.0 s versus rupture distance from horizontal components of the Wenchuan earthquake records in different subareas and for different site conditions, and fitting attenuation curves. (a) Hanging wall area; (b) footwall area; (c) forward directivity area; (d) backward directivity area.

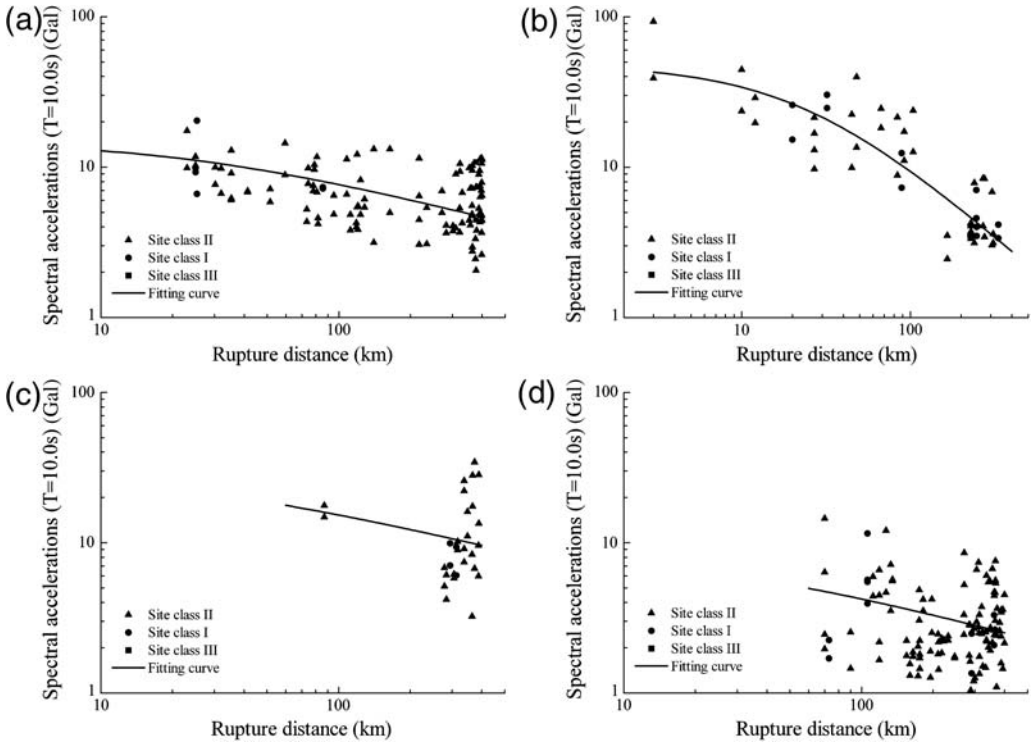

Figure 8. Spectral accelerations at period of 10.0 s versus rupture distance from horizontal components of the Wenchuan earthquake records in different subareas and for different site conditions, and fitting attenuation curves. (a) Hanging wall area; (b) footwall area; (c) forward directivity area; (d) backward directivity area.

There are not clear differences found among the ground motions from the stations with site classes I, II, and III.

Statistical Analysis of the Strong-Motion Records

The number of observed records from the stations with site classes I and III is not enough to analyze the attenuation characteristics of the ground motions. On the other hand, the difference of the ground motions is not clearly found among the records at site class II and site classes I, III in Figures 4–8. Therefore, only the records from the stations with site class II are analyzed in detail in this study.

Peak ground accelerations and spectral accelerations versus rupture distance used in this study from the ground motion records at site class II are shown in Figures 4–8 and Figures 9–13(a). The attenuations of the peak ground acceleration and spectral accelerations at periods of 0.3 s, 1.0 s, 3.0 s, and 10 s are studied in different subareas; the corresponding fitting attenuation curves are shown in Figures 4–8 and Figures 9–13(b). In the statistical analysis, the following

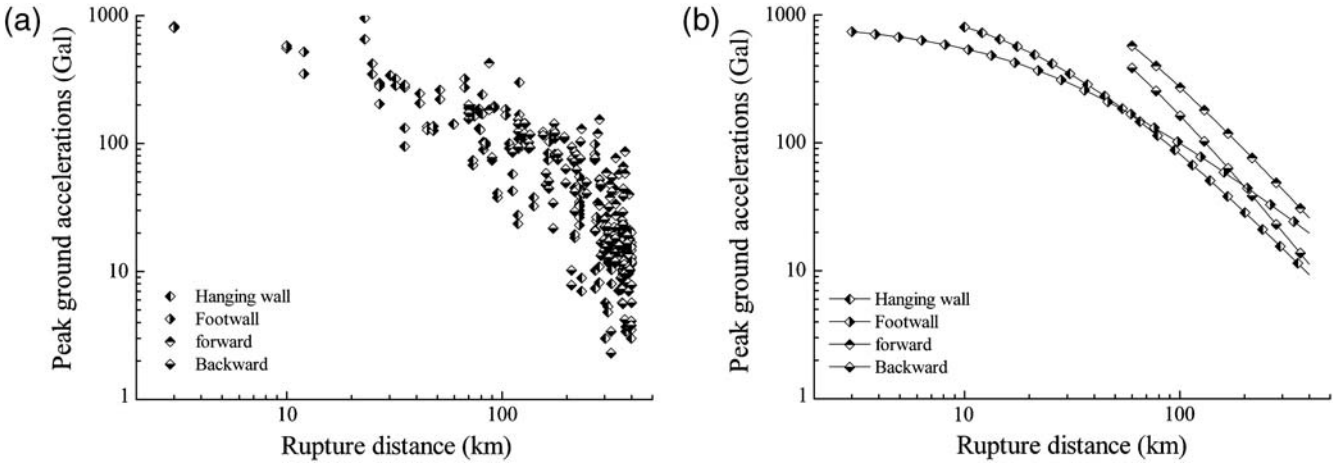

Figure 9. Peak ground accelerations versus rupture distance and relative fitting curves of attenuation relations for horizontal components of the Wenchuan earthquake records in different subareas and for site class II. (a) Observed data; (b) fitting curve of attenuation relations.

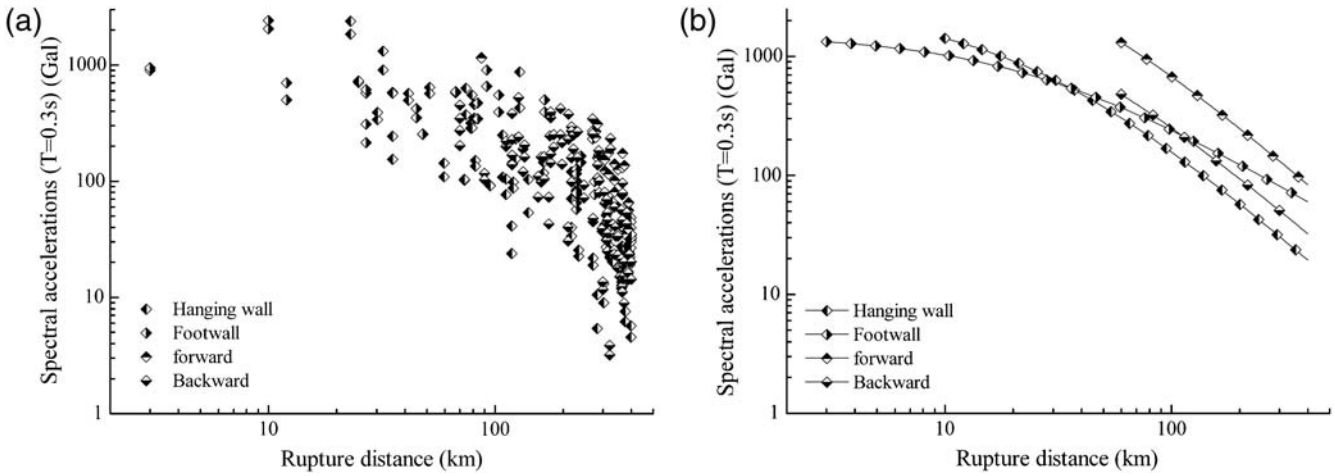

Figure 10. Spectral accelerations at spectral period of 0.3 s versus rupture distance and relative fitting curves of attenuation relations for horizontal components of the Wenchuan earthquake records in different subareas and for site class II. (a) Observed data; (b) fitting curve of attenuation relations.

formula is used to describe the attenuation relations of the peak ground acceleration and spectral accelerations:

$$\log(Y) = C_1 + C_2 \log(R + C_3), \qquad (1)$$

where Y is the peak ground acceleration or spectral acceleration, R is the rupture distance, and C_1, C_2, and C_3 are the regression coefficients.

Comparison of the Peak Ground Acceleration and Spectral Acceleration Attenuations in the Four Subareas

Figures 9 and 10 show the regression curves of attenuation relations for the peak ground acceleration and spectral acceleration at the period of 0.3 s versus rupture distance in the four subareas, including the hanging wall area, footwall area, forward directivity area, and backward directivity area. The peak ground acceleration and spectral acceleration at the period of 0.3 s are considerably larger in the forward directivity area than in the other subareas, and in the near-fault area (the rupture distance within 40 km), the peak ground acceleration and spectral acceleration at the period of 0.3 s are clearly larger in the hanging wall area than in the footwall area, but an opposite trend appears in the range of rupture distances over 40 km. The results indicate that there exists a strong forward directivity effect and hanging wall/footwall effect for the peak ground acceleration, but the effects decrease with an increase of rupture distance.

Figures 11–13 show the regression curves of attenuation relations for spectral accelerations at periods of 1.0 s, 3.0 s, and 10.0 s versus rupture distances in the four subareas. Spectral accelerations in the forward directivity area are considerably larger than those in the other subareas; furthermore, the differences increase with an increase of rupture distance. The results indicate that there exists a strong forward directivity effect, but the hanging wall/footwall effect disappears in spectral accelerations at periods of 1.0 s, 3.0 s, and 10.0 s,

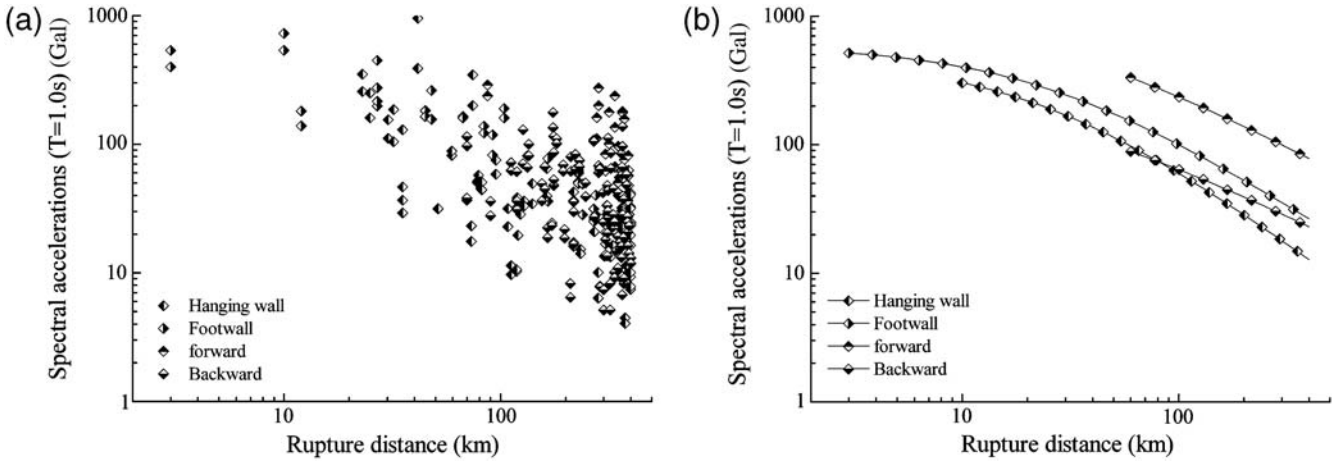

Figure 11. Spectral accelerations at spectral period of 1.0 s versus rupture distance and relative fitting curves of attenuation relations for horizontal components of the Wenchuan earthquake records in different subareas and for site class II.

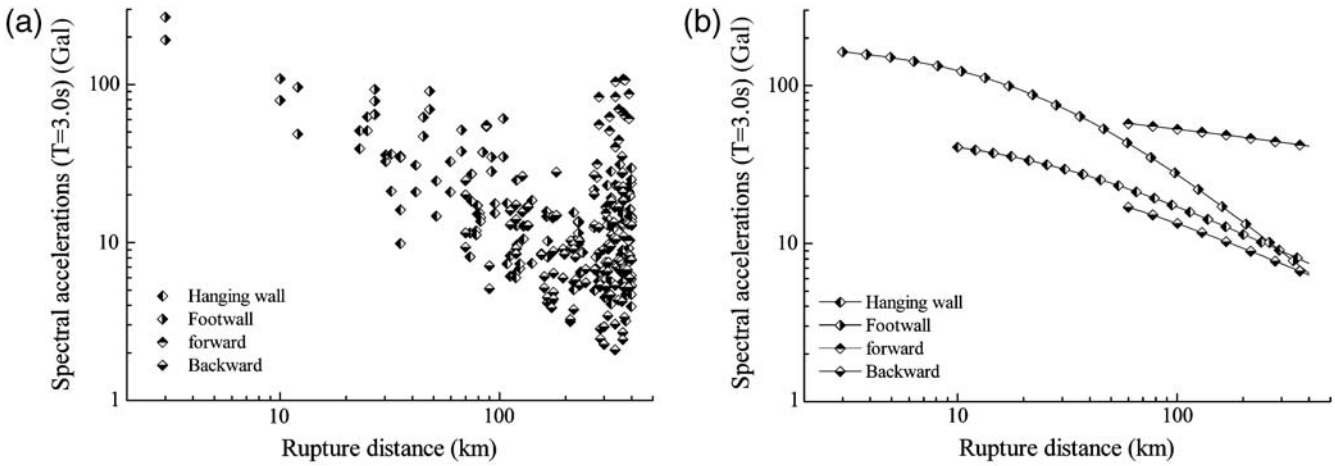

Figure 12. Spectral accelerations at spectral period of 3.0 s versus rupture distance and relative fitting curves of attenuation relations for horizontal components of the Wenchuan earthquake records in different subareas and for site class II. (a) Observed data; (b) fitting curve of attenuation relations.

even if in the near-fault area an opposite trend is found, that is, the spectral accelerations are smaller in the hanging wall area than in the footwall area. Figure 13 also shows that the spectral acceleration at the period of 10 s is larger in the hanging wall area than in the footwall area in the range of rupture distances over 100 km, but an opposite trend appears in the range of rupture distances within 100 km. The results indicate that the hanging wall/footwall effect disappears with an increase of the period; furthermore, an opposite effect appears for spectral accelerations at long period.

Comparison of Peak Ground Accelerations and Spectral Accelerations at Different Spectral Periods

Some research results presented previously are based on the attenuations of the peak ground acceleration and spectral accelerations at periods of 0.3 s, 1.0 s, 3.0 s, and 10.0 s, respectively. Some results seem to show the opposite trends for the peak ground acceleration and different spectral accelerations. Here, further comparison is presented of the peak ground acceleration and spectral accelerations at different periods.

Figure 14 shows the attenuation curves of the peak ground acceleration and spectral accelerations at periods of 0.3 s, 1.0 s, 3.0 s, and 10.0 s for the Wenchuan earthquake ground motions in different subareas. The attenuation degree of spectral accelerations versus rupture distance decreases with the increase of spectral period; the attenuation degree of the peak ground acceleration is almost the same as that at the period of 0.3 s, except in the backward directivity area. It is found that the spectral acceleration at the long period of over 3.0 s has almost no decrease in forward directivity area. This phenomenon is judged not to be induced by the forward rupture directivity and simply by the site condition (site classes), but rather by the basin effect. Because most of the stations in the forward directivity area are located in the area

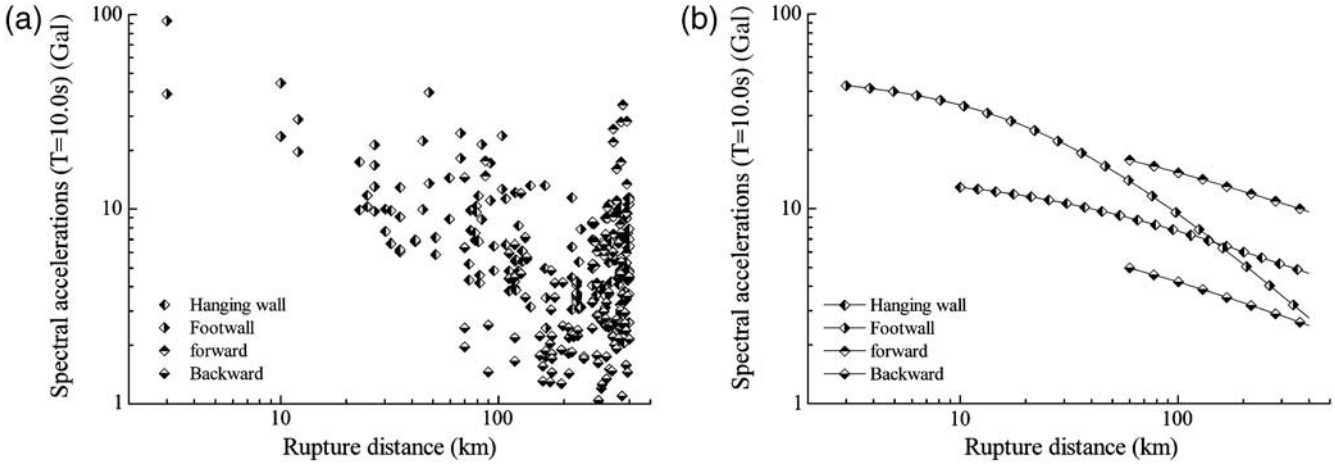

Figure 13. Spectral accelerations at spectral period of 10.0 s versus rupture distance and relative fitting curves of attenuation relations for horizontal components of the Wenchuan earthquake records in different subareas and for site class II. (a) Observed data; (b) fitting curve of attenuation relations.

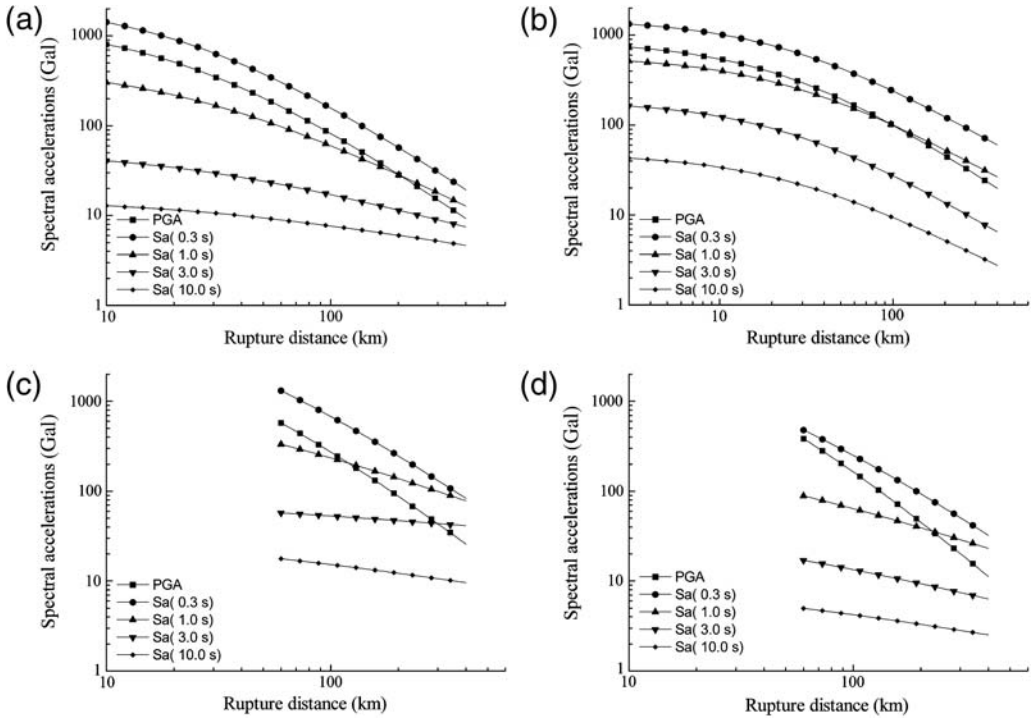

Figure 14. Attenuation curves of peak ground acceleration and spectral accelerations at periods of 0.3 s, 1.0 s, 3.0 s, and 10.0 s for the Wenchuan earthquake ground motions in different subareas. (a) Hanging wall area; (b) footwall area; (c) forward directivity area; (d) backward directivity area.

of the Weihe basin, the components of ground motions in the long period range might be significantly amplified by the basin effect of the Weihe basin.

Comparison of the Observed Attenuation Curves and the Predicted Attenuation Curves by an Empirical Attenuation Model

The attenuation curves of observed ground motions from the Wenchuan earthquake are compared with the predicted ones by an empirical attenuation model (M_w 7.9). The empirical attenuation model presented by Campbell and Bozorgnia (2008) is used in this study. Because the shallow site response term in the empirical attenuation model is related to the special site condition of each station, the site response term is not considered in this study. Figure 15 shows that the peak ground accelerations of observed ground motions are very much larger than those predicted by the Campbell and Bozorgnia (2008) attenuation model, but an opposite trend appears in the attenuation curves of spectral

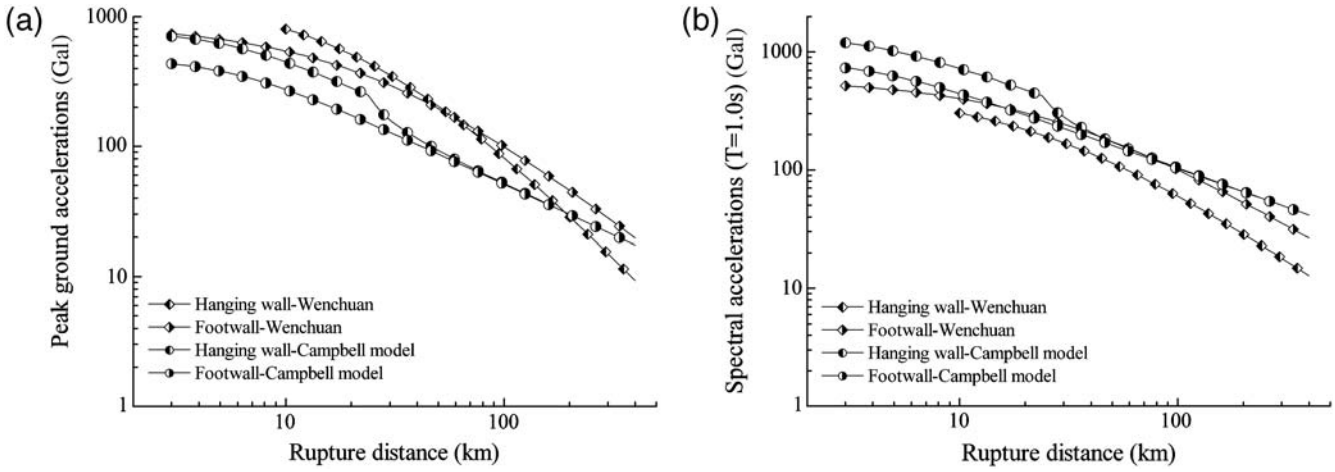

Figure 15. Comparison of attenuation curves of peak ground accelerations and spectral accelerations between the observed ground motions and predicted ground motions by the Campbell and Bozorgnia (2008) attenuation model. (a) Attenuation curves of peak ground accelerations; (b) attenuation curves of spectral accelerations at periods of 1.0 s.

accelerations at periods of 1.0 s. The predicted peak ground accelerations have the same trends of the hanging wall/footwall effects as the observed ones; a strong hanging wall/footwall effect of spectral accelerations at the period of 1.0 s is also predicted by the Campbell and Bozorgnia (2008) attenuation model, but the effect is not found in observed ground motion.

Conclusion

The hanging wall/footwall effects, directivity effects, and attenuation characteristics of ground motions from the Wenchuan earthquake are analyzed based on a number of strong-motion records in the range of rupture distance within 400 km, and some characteristics of ground motions are revealed. It is found that:

1. A clear hanging wall/footwall effect appears in near-fault ground motions within a rupture distance of 40 km, but it only appears in the peak ground acceleration and components at short periods below 1.0 s, and the hanging wall/footwall effect disappears in spectral accelerations with an increase of the spectral period; furthermore, an opposite effect appears for spectral accelerations at the long period.
2. A strong forward directivity effect appears in ground motions over the whole range of rupture distance and spectral period; the peak ground acceleration and spectral accelerations are significantly larger in the forward directivity area than in other areas in the range of rupture distance over 50 km.
3. The attenuation degree of spectral accelerations versus rupture distance decreases with the increase of the spectral period.
4. The peak ground accelerations of observed ground motions are very much larger than those predicted by the Campbell and Bozorgnia (2008) attenuation model, but an opposite trend appears in the spectral accelerations at periods of 1.0 s.

Because of complicated fault rupture processes and site conditions including topography, soil layers, and basin, attenuation relations of ground motions must be complex. Therefore, a more detailed study of the records from the mainshock and aftershocks will be conducted on the study of ground motions from the Wenchuan earthquake in the future.

Data and Resources

The strong-motion records used in this study were provided by the China Strong-Motion Net Center. The files for all records can be obtained from the China Strong-Motion Net Center at www.csmnc.net (last accessed August 2009).

Acknowledgments

The records used in this study are provided by the National Strong-Motion Networks Center of China. We give our thanks to the National Strong-Motion Networks Center of China and all of the relevant managers and experts. This research work is also supported by the National Natural Science Foundation of China (90715038) and the National Basic Research Program of China (2007CB71420).

References

Campbell, K. W., and Y. Bozorgnia (2008). NGA ground motion model for the geometric mean horizontal component of PGA, PGV, PGD and 5% damped linear elastic response spectra for periods ranging from 0.01 to 10 s, *Earthquake Spectra* **24,** no. 1, 139–171.

Earthquake Disaster Prevention and Mitigation Division of CEA (2008). Engineering and Technical Reports on China Digital Strong-Motion Observation Network, *Project inspection report, 2008* (in Chinese).

Gao, G., H. Yu, and S. Li (2001). Strong-motion observations in mainland China, *World Info. Earthquake Eng.* **17,** no. 4, 13–18 (in Chinese with English abstract).

Li, X., and M. Huang (2006). Strong-Motion Project in China—Goals, Strategy and Status, *NSF-CUREE Workshop on Strong-Motion Research Needs and Opportunities*, Oakland, California, October 19–20, 2006.

Li, X., Z. Zhou, M. Huang, R. Wen, H. Yu, D. Lu, Y. Zhou, and J. Cui (2008). Preliminary analysis of strong-motion recordings from the magnitude 8.0 Wenchuan, China earthquake of May 12, 2008, *Seismol. Res. Lett.* **79,** no. 6, 844–854.

Li, X., Z. Zhou, H. Yu, R. Wen, D. Lu, M. Huang, Y. Zhou, and J. Cui (2008). Strong motion observations and recordings from the great Wenchuan earthquake, *Earthquake Eng. Eng. Vib.* **7,** no. 3, 235–246.

Nozu, A. (2004). Current status of strong-motion earthquake observation in Japanese ports, *J. Japan Assoc. Earthquake Eng.* **4,** no. 3 (Special Issue), 79–83.

Wang, W., L. Zhao, J. Li, and Z.-X. Yao (2008). Rupture process of the M_s 8.0 Wenchuan earthquake of Sichuan, China, *Chin. J. Geophys.* **51,** no. 5, 1403–1410 (in Chinese with English abstract).

Xu, X., X. Wen, G. Yu, G. Chen, Y. Klinger, J. Hubbard, and J. Shaw (2009). Coseismic reverse- and oblique-slip surface faulting generated by the 2008 M_w 7.9 Wenchuan earthquake, China, *Geology* **37,** no. 6, 515–518.

Xu, X., G. Yu, G. Chen, Y. Ran, C. Li, Y. Chen, and C. Chang (2009). Parameters of coseismic reverse- and oblique-slip surface ruptures of the 2008 Wenchuan earthquake, eastern Tibetan Plateau, *ACTA Geol. Sin.* **83,** no. 4, 673–684.

Zhou, Y. (2006). Strong-motion observation in mainland China, *Recent Developments in World Seismology* 2006, no. 11, 1–6 (in Chinese with English abstract).

Institute of Geophysics
China Earthquake Administration
5 Minzu Xueyuan Nan Road
Beijing 100081, China
beerli@vip.sina.com
(X.J.L.)

Institute of Engineering Mechanics
China Earthquake Administration
Harbin, China
(L.L., Y.S.W., T.Y.)

Manuscript received 31 August 2009